PROCEEDINGS, 43rd Workshop on Geothermal Reservoir Engineering
Stanford University, Stanford, California, February 12-14, 2018
SGP-TR-213

Using Borehole Induced Structure Measurements at Fallon FORGE Combined with Numerical Modeling to Estimate In-Situ Stresses

Derrick J. Blanksma[1], Kelly Blake[2], Will Pettitt[1], Andrew Sabin[2], Varun Varun[1] and Branko Damjanac[1]

[1]Itasca Consulting Group 111 Third Ave South Suite 450 Minneapolis MN 55401

[2]U.S. Navy Geothermal Program Office

dblanksma@itascacg.com

Keywords: EGS, FORGE, borehole breakouts, *3DEC*, in-situ stresses

ABSTRACT

Understanding the in-situ stress state is an important component for all subsurface engineering disciplines. In Enhanced Geothermal Systems (EGS) the behavior of joints, fractures and faults during hydraulic stimulation depends on the principal stress field at depth. In this study, we take an alternative approach to interpreting the stress field by generating a three-dimensional (3D) distinct element model in *3DEC* that simulates a borehole at the Fallon FORGE site where breakouts have been measured at the depth of the proposed EGS reservoir.

The simulated breakouts that develop in the 3D geomechanical model depend on the input principal stress magnitudes, strength of the rock, and orientation of the borehole. Assuming the strength of the rock is known, we compare the locations of simulated breakouts to the observed breakouts at different input stresses to produce a range for the likely in-situ stress magnitudes. The range is further informed by an analysis of observed stability on joints, fractures and faults under in-situ stress conditions. The approach illustrates that an ability to simulate where a borehole breakout occurs can provide confidence in estimating the magnitude of the principal stresses that supports traditional measurements of stress at depth.

Estimates for the in-situ stresses at Fallon FORGE were produced for different rock strengths to test uncertainties. The results indicate a minimum horizontal stress that lies in a range of 53% to 79% of the vertical stress and maximum horizontal stress that lies in a range of 79% to 88% of the vertical stress. Using this approach, the best estimate of the minimum and maximum horizontal principal stresses at the Fallon FORGE site are 56% and 80% of the vertical stress, respectively.

1. INTRODUCTION

The Department of Energy (DOE)'s Frontier Observatory for Research in Geothermal Energy (FORGE) project at Fallon is currently collecting and analyzing geomechanical, geophysical, geologic and borehole data for Phase 2B. The purpose is to gain an analytically thorough understanding of the potential EGS reservoir at depth. With the aid of a corehole currently being drilled into the proposed reservoir, stress magnitude and more stress orientation data will be available. However, for the purpose of mechanical modelling throughout Phase 2B prior to the drilling of the corehole, stress magnitudes needed to be estimated. Previous work on image logs from the FOH-3D borehole drilled within the Fallon FORGE site provided a data set that could be utilized for accurate stress magnitude estimation for use in geomechanical and reservoir stimulation models.

Determining the principal stress characteristics from borehole breakouts has been well established and is commonly used in scientific applications, e.g. Moos and Zoback (1990), Zajac and Stock (1997), and Zoback et al. (2003). Breakout data can predict quite accurately the orientation of the horizontal principal stresses; however, uncertainty arises when trying to calculate the principal stress magnitudes. The approach involves detailed knowledge of the cross-sectional shape of the breakout and, assuming a strength criterion, one can calculate the horizontal stress magnitudes, e.g. Zoback, et al. (1985). The difficulty lies in determining the exact shape of the breakout. For example, if one measured a breakout's half-span to be 20° (a typical breakout span) and measured the ratio of the breakout depth to the borehole radius to be 1.02 ± 0.5%, the uncertainty in the stress measurements could be as high as 50% (Figure 1).

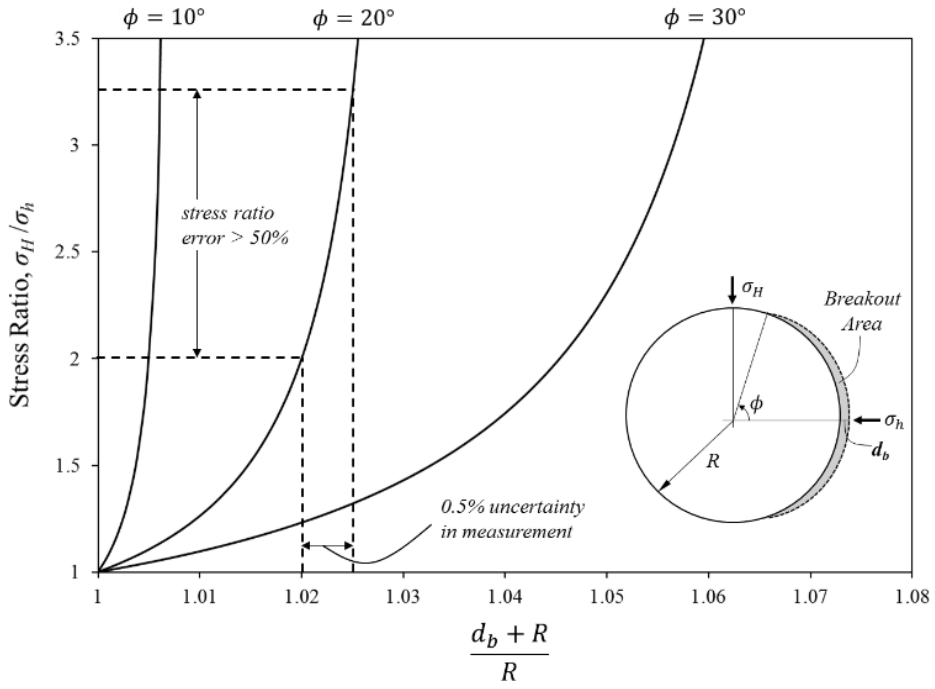

Figure 1: Stress ratio (σ_H/σ_h) as a function of breakout depth (d_b) for three different breakout half-spans (ϕ). A small error in the measured breakout depth can lead to unreasonably large stress ratio's e.g. Zoback et al. (1985).

Downhole geophysical instruments such as ultrasonic borehole televiewers (BHTV) provide high resolution images of the breakout shape, however determining the span and depth of the breakout can lead to unreasonably large stress estimations. Additionally, the problem becomes even more difficult if the well is deviated, e.g. Mastin (1988).

This study aims to utilize breakout and fracture data along the length of a borehole to help constrain the magnitude of the horizontal in-situ stresses.

2. BOREHOLE FOH-3D

The borehole simulated in *3DEC* has the same characteristics as the FOH-3D borehole located on the Fallon FORGE site at 36˚23'8.56"N, 118˚40'22.68"W. FOH-3D was drilled by the Navy Geothermal Program Office on the Naval Air Station Fallon within the Carson Sink of Nevada; the current location of one of the Department of Energy's funded FORGE projects. The borehole yielded a great amount of data and furthered the understanding of the temperature gradients within the Carson Sink. FOH-3D reached a maximum temperature of 150˚C with a temperature gradient of 80˚C/km.

FOH-3D was drilled to 2743 meters in 2006. FOH-3 was initially drilled to a depth of 2134 meters in August 1993. When it was deepened in 2006, it was determined that the upper section of the extension was highly deviated. The maximum deviation in FOH-3D is approximately 27°.

FOH-3D was chosen for this analysis due to breakouts recorded within the proposed EGS reservoir of the Mesozoic crystalline basement. These breakouts were part of an overall induced structure analysis were investigated in the FOH-3D borehole, e.g. Blake and Davatzes (2012), Blake et al., (2015). The induced structures identified and analyzed within image logs from FOH-3D and the proximal 61-36 borehole yielded an average maximum horizontal principal stress oriented 11° from North. The well trace of FOH-3D, as well as the generalized stratigraphic column, is shown in Figure 2.

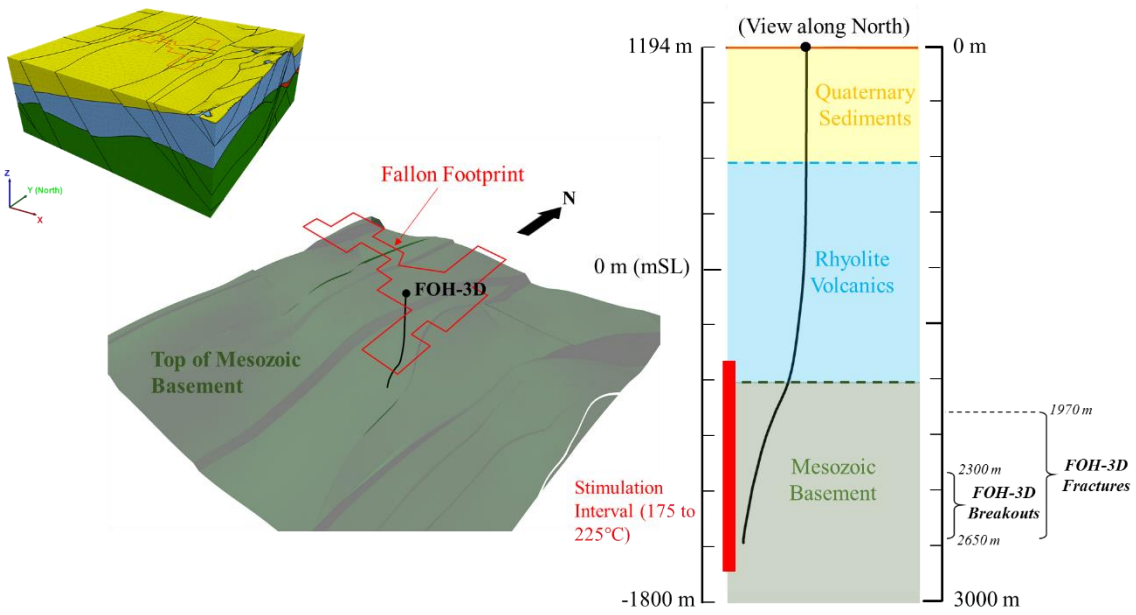

Figure 2: Location of borehole FOH-3D at the Naval Air Station Fallon site and the generalized stratigraphic column. The location of breakout and fracture data relevant to this study are shown at their respective depths. The top of the Mesozoic basement unit is shown in the oblique view (middle) as well as the stratigraphic column (right).

3. ESTIMATION OF THE IN-SITU STRESSES

Estimating the magnitudes of the in-situ stresses was a three-part approach that uses, (1) FOH-3D breakouts, and, (2) FOH-3D fracture orientations to constrain the stress magnitude range. The final part (3) compared the in-situ stress range developed in parts (1) and (2) to known stress measurement in the Carson Sink region.

3.1 Borehole Stability

In order to determine if a breakout is possible at a certain point along the borehole, we must calculate the maximum stresses (compression positive) at the borehole wall taking into account its non-vertical orientation. The elastic solution to this problem has been solved before, e.g. Mastin (1988), Peska and Zoback (1995). The solution presented here is provided to add clarity and show how stresses develop along FOH-3D at Fallon FORGE.

A perfectly vertical borehole subjected to horizontal in-situ stresses will perturb the stress field according to the classic Kirsch solution for a circular hole in an elastic medium, e.g. Kirsch (1898). If we align one of the axes along the maximum horizontal stress (σ_H) and measure counter-clockwise by and angle θ in the horizontal plane, we find the maximum and minimum values of stress at the borehole wall are $3\sigma_H - \sigma_h$ when $\theta = \pi/2$ or $\theta = 3\pi/2$ and $3\sigma_h - \sigma_H$ when $\theta = 0$ or $\theta = \pi$, e.g. Jaeger and Cook (2007). Expanding on the same principal of the Kirsch solution to a deviated borehole requires a series of coordinate transformations from the geographic coordinate system to the borehole coordinates,

$$\boldsymbol{G} = \boldsymbol{RBR}^{\boldsymbol{T}} \tag{1}$$

where $\boldsymbol{B}$, $\boldsymbol{R}$, $\boldsymbol{G}$ are the borehole stress tensor, rotation matrix and geographic stress tensor, respectively. Once the borehole stresses are determined we can rewrite the stresses in their polar components as the radial, tangential and axial stresses ($\sigma_{rr}, \sigma_{\theta\theta}, \sigma_{zb}$). Finally, the maximum and minimum effective stresses can be determined on the borehole wall from the polar stress components. It will be shown that a breakout is influenced by the orientation of the borehole and the relative magnitude of the in-situ stresses.

First, the normal and shear stresses are retrieved for a given depth in the model's geographic coordinate system (i.e. the XYZ axis is aligned with East, North and Vertical). The transformation to the borehole coordinate system is as follows,

$$\begin{bmatrix} x^b \\ y^b \\ z^b \end{bmatrix} = \boldsymbol{R}^{\boldsymbol{T}} \begin{bmatrix} X \\ Y \\ Z \end{bmatrix} \tag{2}$$

where (x^b, y^b, z^b) and $\boldsymbol{R}$ are the borehole coordinates and coordinate rotation matrix, respectively. To determine the borehole stress tensor, we can rearrange (1) to be,

$$\boldsymbol{B} = \boldsymbol{R}^{\boldsymbol{T}}\boldsymbol{G}\boldsymbol{R} \tag{3}$$

$$\boldsymbol{R} = \begin{bmatrix} \cos\phi\cos\delta & -\cos\phi\sin\delta & -\sin\phi \\ \sin\delta & \cos\delta & 0 \\ \sin\phi\cos\delta & -\sin\phi\sin\delta & \cos\phi \end{bmatrix} \tag{4}$$

where angles δ and ϕ are the boreholes trend measured clockwise from north and angular deviation from the vertical axis, respectively. The rotation matrix ($\boldsymbol{R}$) is derived from a series of two rotations about the geographic coordinate system. Figure 3 shows how the rotation matrix is produced.

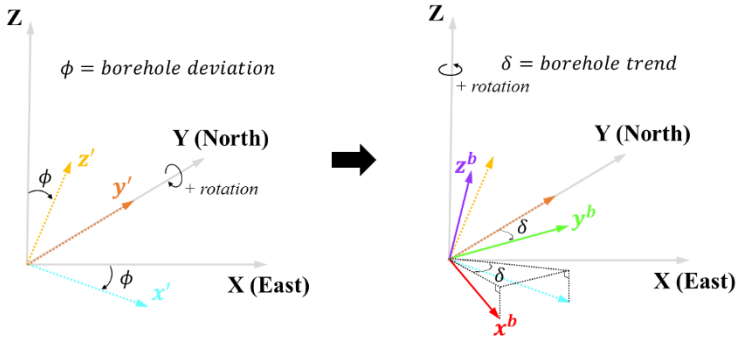

$$R_Y(\phi) = \begin{bmatrix} cos\phi & 0 & -sin\phi \\ 0 & 1 & 0 \\ sin\phi & 0 & cos\phi \end{bmatrix} \qquad R_Z(\delta) = \begin{bmatrix} cos\delta & -sin\delta & 0 \\ sin\delta & cos\delta & 0 \\ 0 & 0 & 1 \end{bmatrix}$$

$$\boldsymbol{R} = R_Y(\phi)R_Z(\delta) = \begin{bmatrix} cos\phi cos\delta & -cos\phi sin\delta & -sin\phi \\ sin\delta & cos\delta & 0 \\ sin\phi cos\delta & -sin\phi sin\delta & cos\phi \end{bmatrix}$$

Figure 3: Rotation matrix ($\boldsymbol{R}$) that transforms the geographic stress tensor ($\boldsymbol{G}$) to the local borehole stress tensor ($\boldsymbol{B}$).

Note in Figure 3, $\boldsymbol{z^b}$ points upward along the borehole axis. Considering the addition of pore pressure, the final stress state on the borehole wall (in borehole coordinates) is,

$$\sigma' = \boldsymbol{B} - \delta_{ij}\boldsymbol{P_p} \tag{5}$$

where σ', δ_{ij}, $\boldsymbol{P_p}$ are the effective borehole stress tensor, Kronecker delta function, and pore pressure.

The borehole coordinate system is right-handed, cartesian and often it is helpful to express the stresses at the borehole wall in terms of polar coordinates. The derivation of the borehole stresses to polar coordinates are not shown here, however, other sources have derived these formulae, e.g. Hiramatsu and Oka (1962), Hayes (1965), Fairhurst (1967):

$$\sigma_{zb} = \sigma'_{33} - 2\upsilon(\sigma'_{11} - \sigma'_{22})\cos 2\theta - 4\upsilon\sigma_{12}\sin 2\theta \tag{6}$$

$$\sigma_{\theta\theta} = \sigma'_{11} + \sigma'_{22} - 2\upsilon(\sigma'_{11} - \sigma'_{22})\cos 2\theta - 4\upsilon\sigma_{12}\sin 2\theta \tag{7}$$

$$\tau_{\theta z} = 2(\sigma_{23}\cos\theta - \sigma_{13}\sin\theta) \tag{8}$$

$$\sigma_{rr} = \Delta P \tag{9}$$

$$\tau_{r\theta} = 0 \tag{10}$$

where σ_{zb}, $\sigma_{\theta\theta}$, $\tau_{\theta z}$, σ_{rr}, $\tau_{r\theta}$, θ, ν, ΔP are the axial stress, tangential stress, shear stress in the θ-z plane, radial stress, shear stress in the r-θ plane, azimuth measured counter-clockwise from the boreholes x-axis (x_b), Poisson ratio, and the difference between wellbore fluid pressure and the surrounding rock pore pressure. The tangential stress ($\sigma_{\theta\theta}$) acts at the borehole wall and varies as a function of θ. If z_b was aligned with a principal stress, the maximum and minimum tangential stresses can be derived from the Kirsch solution based only on

the other two principal stresses. However, due to the deviation in the borehole the axial component (σ_{zb}) of stress also influences the minimum and maximum stresses on the borehole wall.

Consider each point along the boreholes azimuth that lies on a plane tangent to the borehole wall that contains the normal and axial stresses ($\sigma_{\theta\theta}$, σ_{zb}) (see Figure 4).

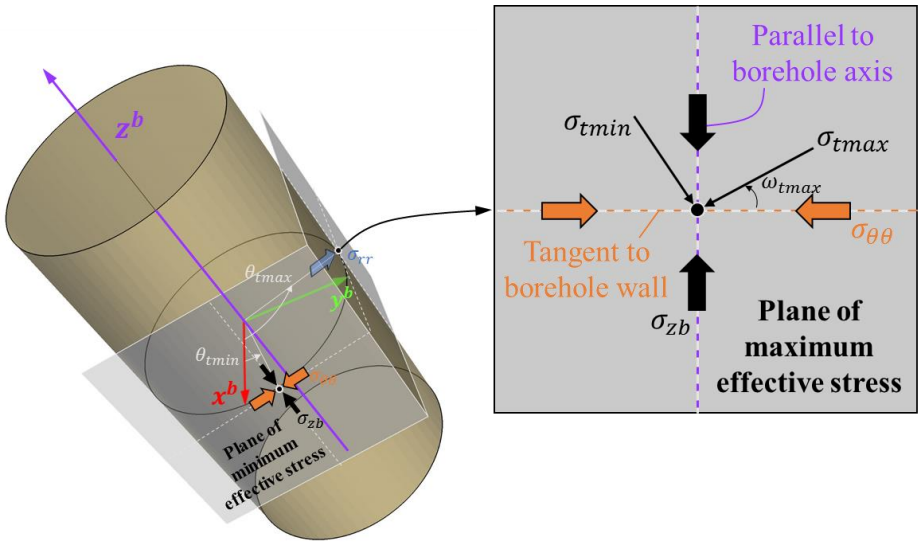

Figure 4: Left: Stresses on the wall of a deviated borehole. The boreholes coordinate system is x^b, y^b and z^b. The planes of maximum and minimum effective stress are tangent to the borehole wall located at θ_{tmax} and θ_{tmin}, respectively. Right: Plane of maximum effective stress – the maximum (σ_{tmax}) and minimum (σ_{tmin}) effective stresses act along this plane rotated counter-clockwise be an angle ω_{tmax}. If σ_{tmax} exceeds the compressive strength of the rock a breakout can form.

There exists a plane tangent to the borehole wall at which the maximum effective stress is located (σ_{tmax}). Similarly, there also exists a plane in which the minimum stress is located (σ_{tmin}). The minimum stress can be compressive (+) or tensile (-). The planes of maximum and minimum effective stress are located along the boreholes azimuth at θ_{tmax} and θ_{tmin} , respectively. It is important to note, that while the plane of maximum effective stress contains both a maximum *and* minimum effective stress component, it does not contain the least minimum effective stress. The least minimum effective stress is located on the plane of minimum effective stress at a different azimuth (θ_{tmin}) along the borehole (see Figure 4).

Now we can resolve the stresses only on the plane of maximum effective stress. The normal stresses on this plane are $\sigma_{\theta\theta}$ and σ_{zb}, which are mutually orthogonal and define a set of base coordinates on the plane. Thus, any normal and shear stresses acting on this plane at any point rotated counter-clockwise from the $\sigma_{\theta\theta}$ axis is defined by,

$$\sigma = \frac{1}{2}(\sigma_{\theta\theta} + \sigma_{zb}) + \frac{1}{2}(\sigma_{\theta\theta} - \sigma_{zb})\cos 2\omega + \tau_{\theta z}\sin 2\omega \tag{11}$$

$$\tau = \frac{1}{2}(\sigma_{zb} - \sigma_{\theta\theta})\sin 2\omega + \tau_{\theta z}\cos 2\omega \tag{12}$$

where σ, τ, ω are the normal stress, shear stress and angle of rotation w.r.t. $\sigma_{\theta\theta}$. The maximum and minimum stresses (σ_{tmax}, σ_{tmin}) acting on the plane are rotated by ω_{tmax} counter-clockwise from the $\sigma_{\theta\theta}$ axis. Because these are principal stresses with no shear component we can set (12) to zero and arrive at the following,

$$\tan 2\omega_{t\max} = \frac{2\tau_{\theta z}}{\sigma_{\theta\theta} - \sigma_{zb}} \tag{13}$$

In the general case where $\omega_{tmax} \neq 0$ there are two roots that satisfy (13), lying in the range $0 \leq \omega_{tmax} \leq \pi$. To determine σ_{tmax} we can rewrite the principal stresses in a recognizable way with the aid of the following trigonometric properties:

$$\sin 2\omega_{t\max} = \pm(1+\cot^2 2\omega_{t\max})^{-1/2} = \pm\tau_{\theta z}\left(\tau_{\theta z}^2 + \frac{1}{4}(\sigma_{\theta\theta}-\sigma_{zb})^2\right)^{1/2} \tag{14}$$

$$\cos 2\omega_{t\max} = \pm(1+\tan^2 2\omega_{t\max})^{-1/2} = \pm\frac{1}{2}(\sigma_{\theta\theta}+\sigma_{zb})\left(\tau_{\theta z}^2 + \frac{1}{4}(\sigma_{\theta\theta}-\sigma_{zb})^2\right)^{1/2} \tag{15}$$

Equations (14) and (15) can be substituted into (11) to find the maximum and minimum effective stresses acting in the plane of maximum effective stress,

$$\sigma_{t\max} = \frac{1}{2}(\sigma_{\theta\theta}+\sigma_{zb}) + \left(\tau_{\theta z}^2 + \frac{1}{4}(\sigma_{\theta\theta}-\sigma_{zb})^2\right)^{1/2} \tag{16}$$

$$\sigma_{t\min} = \frac{1}{2}(\sigma_{\theta\theta}+\sigma_{zb}) - \left(\tau_{\theta z}^2 + \frac{1}{4}(\sigma_{\theta\theta}-\sigma_{zb})^2\right)^{1/2} \tag{17}$$

Generally, it is not possible to maximize σ_{tmax} or minimize σ_{tmin} with respect to the borehole azimuth angle θ analytically, e.g. Qian and Pedersen (1991). To determine σ_{tmax}, a numerical solution was obtained by searching for the maximum value in (16) with an angular increment (θ) equal to one degree. Once θ_{tmax} is found to an acceptable degree, it can be substituted into (13) to determine ω_{tmax} in the plane of maximum effective stress.

The same process described above can be used to find the minimum principal stress acting on the borehole wall in the plane of minimum effective stress. A plot of the maximum and minimum effective stresses on the borehole wall as a function of the azimuth around the hole, θ, is shown in Figure 5. This case is near the maximum deviation recorded in FOH-3D at 1900 meters vertical depth below the collar. The borehole orientation and in-situ stresses are given in Table 1.

Table 1: FOH-3D orientation and in-situ stress state at 1900 m vertical depth below the collar.

Trend (ϕ) [°]	Deviation (δ) [°]	Vertical Stress (σ_v) [MPa]	Max Horizontal Stress (σ_H) [MPa]	Min Horizontal Stress (σ_h) [MPa]	Pore Pressure (P_p) [MPa]
257	25	43.7	35.0	24.5	18.4

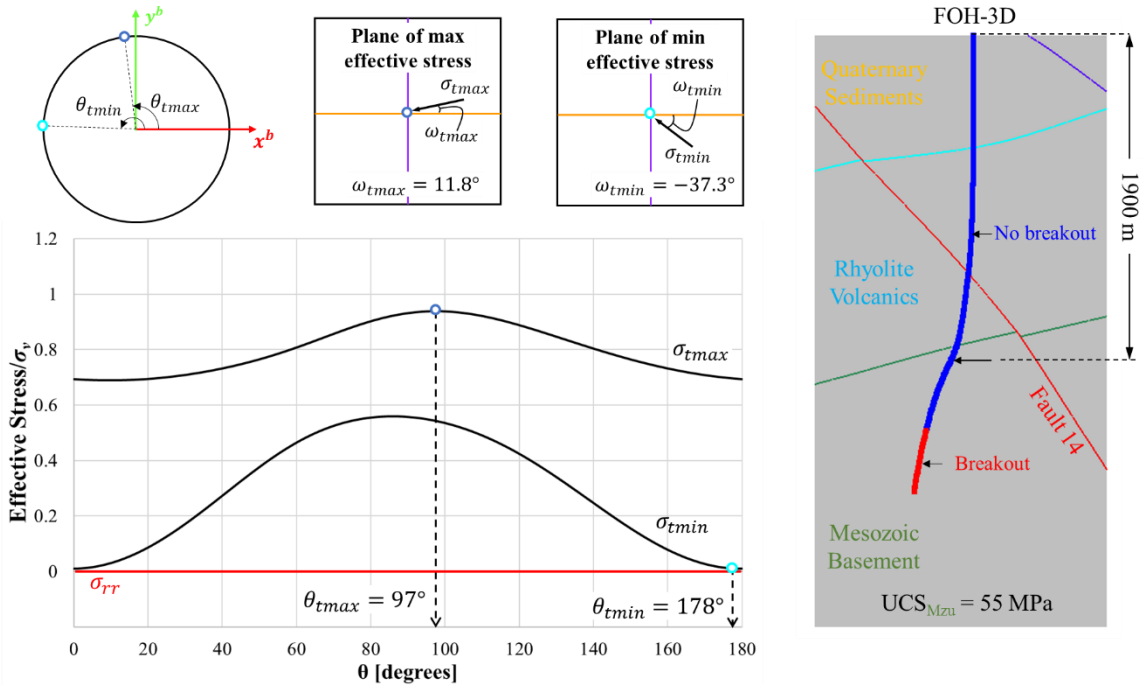

Figure 5: Maximum and minimum stresses on the borehole wall as a function of its azimuth (θ) at 1900 m vertical depth below the collar. The borehole oreintation and in-situ stress state is given in Table 1. The maximum effective stress on the borehole wall is rotated at $\theta_{tmax} = 97°$ and has a magnitude of 41.1 MPa, which does not exceed the compressive strength of 55 MPa, thus a breakout does not occur at this depth.

At 1900 m depth, the maximum compressive stress in borehole FOH-3D is rotated 97° from the boreholes *x*-axis (x^b). The angular rotation in the plane of maximum effective stress (ω_{tmax}) was determined to be 11.8° (see Figure 5). The maximum effective stress on the borehole wall was 41.1 MPa ($0.94\sigma_1$) and the minimum effective stress on the borehole wall was 0.50 MPa ($0.01\sigma_1$). Assuming the compressive strength of the rock at this point on the borehole wall is 55 MPa a breakout would not form. If we analyze a point further down the borehole at 2345 meters vertical depth from the collar, the horizontal stresses increase to a point where a breakout is possible. Table 2 gives the orientation of the borehole and in-situ stresses at 2345 meters vertical depth. Figure 6 shows the resulting stress magnitudes and orientations.

Table 2: FOH-3D orientation and in-situ stress state at 2345 m vertical depth below the collar.

Trend (ϕ) [°]	Deviation (δ) [°]	Vertical Stress (σ_v) [MPa]	Max Horizontal Stress (σ_H) [MPa]	Min Horizontal Stress (σ_h) [MPa]	Pore Pressure (P_p) [MPa]
247	15	55.5	44.4	31.1	22.7

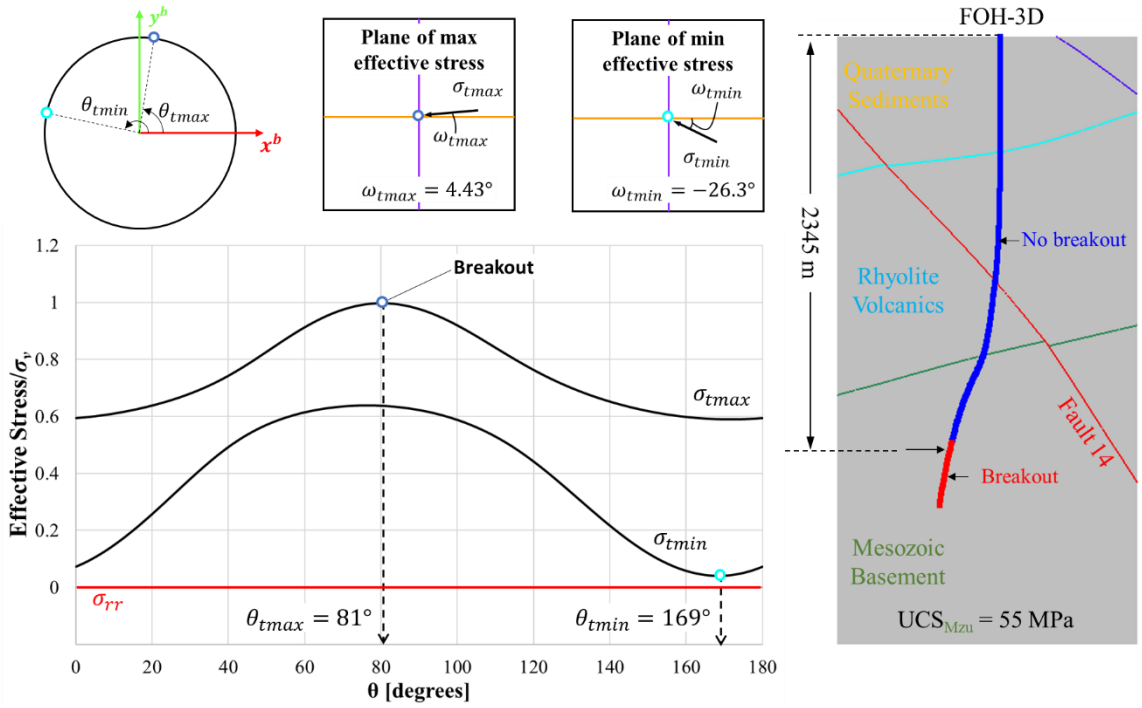

Figure 6: Maximum and minimum stresses on borehole wall as a function of its azimuth (θ) at 2345 meters vertical depth below the collar. The borehole oreintation and in-situ stress state is given in Table 2. The maximum effective stress on the borehole wall is rotated at $\theta_{tmax} = 81°$ and has a magnitude of 55.3 MPa, which does exceed the compressive strength of 55 MPa, thus a breakout can form at this depth.

The breakout stability analysis presented above shows how a breakout can occur on the borehole wall given the in-situ stress state and strength of the rock. However, in the present case, we do not know the magnitudes of the in-situ stresses and we desire to constrain the in-situ stresses based on borehole breakout data.

The first step is to investigate how different in-situ stress states affect breakouts along FOH-3D and compare to actual breakouts recorded from BHTV logs. This step requires some additional assumptions.

1. The in-situ stress regime is considered normal faulting with the maximum principal stress oriented vertically and the magnitude equal to the overburden.

2. The rock strata are homogeneous and isotropic for the three types (i.e., Quaternary Sediments, Rhyolite Volcanics and Mesozoic Basement). The Uniaxial Compressive Strength (UCS) of the rock in the Mesozoic basement was assumed to be 55 MPa†.

3. The pore pressure is assumed to be hydrostatic along the strata column and does not change due to the temperature gradient. The water table was assumed to be 20 m below the surface.

† A UCS equal to 55 MPa could be considered a small value for hard crystalline rock e.g. Deere and Miller (1966). Indirect measurements (i.e., scratch tests) estimated the UCS in the Mesozoic basement rock to be anywhere from 70 to 200 MPa, e.g. Lutz (2010), Lutz (2011). An additional breakout stability analysis with a UCS equal to 70 MPa was also investigated, the results of which are given in the concluding section.

The only remaining variables are the magnitude of the horizontal in-situ stresses. Theoretically, these stresses can be any value as long as $\sigma_v > \sigma_H > \sigma_h$, which is the criteria for a normal faulting regime. This range can be constrained further since σ_v is the overburden stress and the horizontal stresses can be any value that produces breakouts that are consistent with BHTV logs. For example, Figure 7 shows three *3DEC* models (A, B, and C) each with different in-situ stresses. The geographic stresses are calculated in the model considering the undulating stratigraphic layers and the existence of faults in the stratigraphic column. Calculated breakouts (red) are based on the breakout

stability analysis, and recorded breakouts are shown from BHTV logs (offset in black). The calculated breakouts were determined along the borehole length at 1 meter intervals.

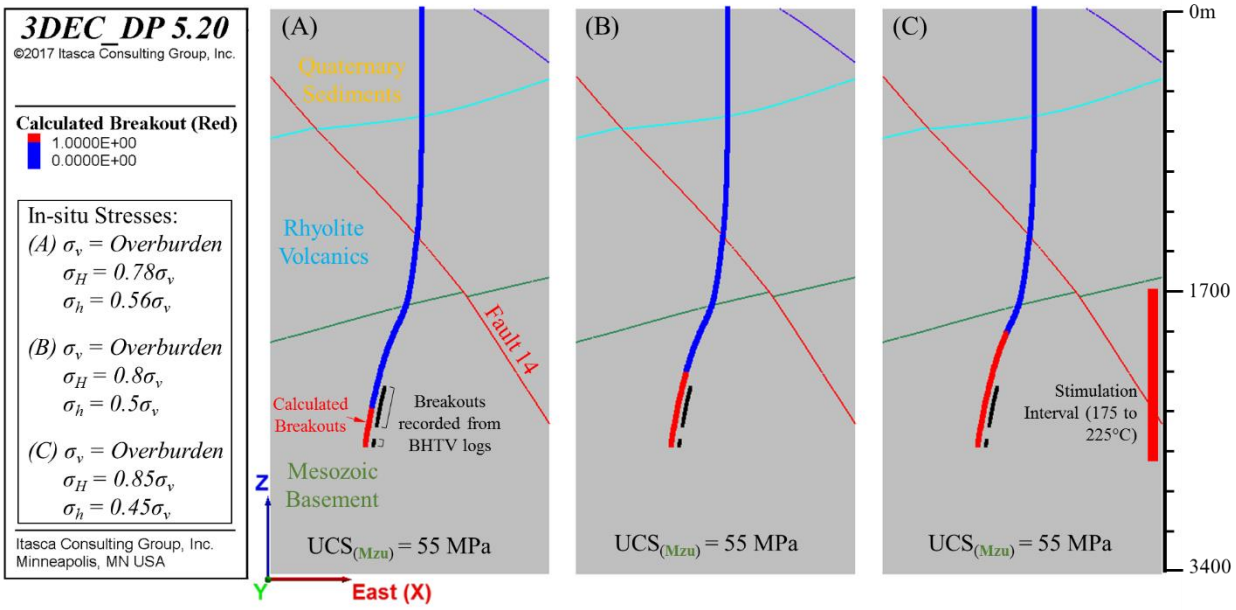

Figure 7: Breakout stability analysis for three different minimum horizontal in-situ stress (σ_h) magnitudes. (A) $\sigma_h = 0.56\sigma_v$: Calculated breakouts fall below the actual recorded breakouts. (B) $\sigma_h = 0.5\sigma_v$: Calculated breakouts occur above the actual recorded breakouts. (C) $\sigma_h = 0.45\sigma_v$: Calculated breakouts occur further above the actual recorded breakouts.

The breakout analysis in Figure 7 suggests that the true in-situ horizontal stresses exist in in the range $0.78\sigma_v < \sigma_H < 0.8\sigma_v$ and $0.5\sigma_v < \sigma_h < 0.56\sigma_v$. However, since σ_h and σ_H are independent variables of each other, it would be impossible to constrain these bounds without additional information.

3.2 Minimum Horizontal In-situ Stress from Fracture Orientations

To further constrain the in-situ stress state at Fallon FORGE, we investigated the potential for slip on pre-existing fractures recorded in the BHTV logs along FOH-3D. From the known fracture orientations and assuming a constant friction angle, the minimum principal stress can be estimated based on the knowledge that these fractures are not in a critical state (i.e., frictional strength is sufficient to keep the fracture from slipping).

First, consider the normal effective stress on a fracture plane:

$$\sigma'_n = \sigma_n - P_p \tag{18}$$

where σ'_n, σ_n, P_p is the normal effective stress, normal stress and pore pressure, respectively. Because the orientation of the fracture planes are known and we assume the maximum principal stress is equal to the overburden, one can calculate the normal stress acting on the fracture plane using a similar coordinate transformation procedure described in Section 3.1. Once the normal stress is determined, the shear behavior is assumed to follow a Coulomb slip criterion with no cohesion:

$$\tau_s = \sigma'_n \tan\theta \tag{19}$$

where τ_s, θ is the shear stress and friction angle on the fracture plane, respectively. In a normal faulting regime, if the minimum horizontal stress is sufficiently small the fracture will slip. Figure 8 shows fractures that can slip for different values of the minimum horizontal stress. The frictional strength is expressed as the friction coefficient ($\mu = tan\theta$) and has an assumed value of 0.84 ($\theta = 40°$). This frictional value is typical of hard rock which commonly lies in the range of 0.6 – 1.0, e.g. Byerlee (1978). Since the potential for fracture slip is determined by the minimum horizontal stress then the maximum horizontal stress was left constant. The slip analysis suggests the least possible value σ_h can be is $0.53\sigma_v$ and this value was considered the lower bound for the minimum horizontal stress range.

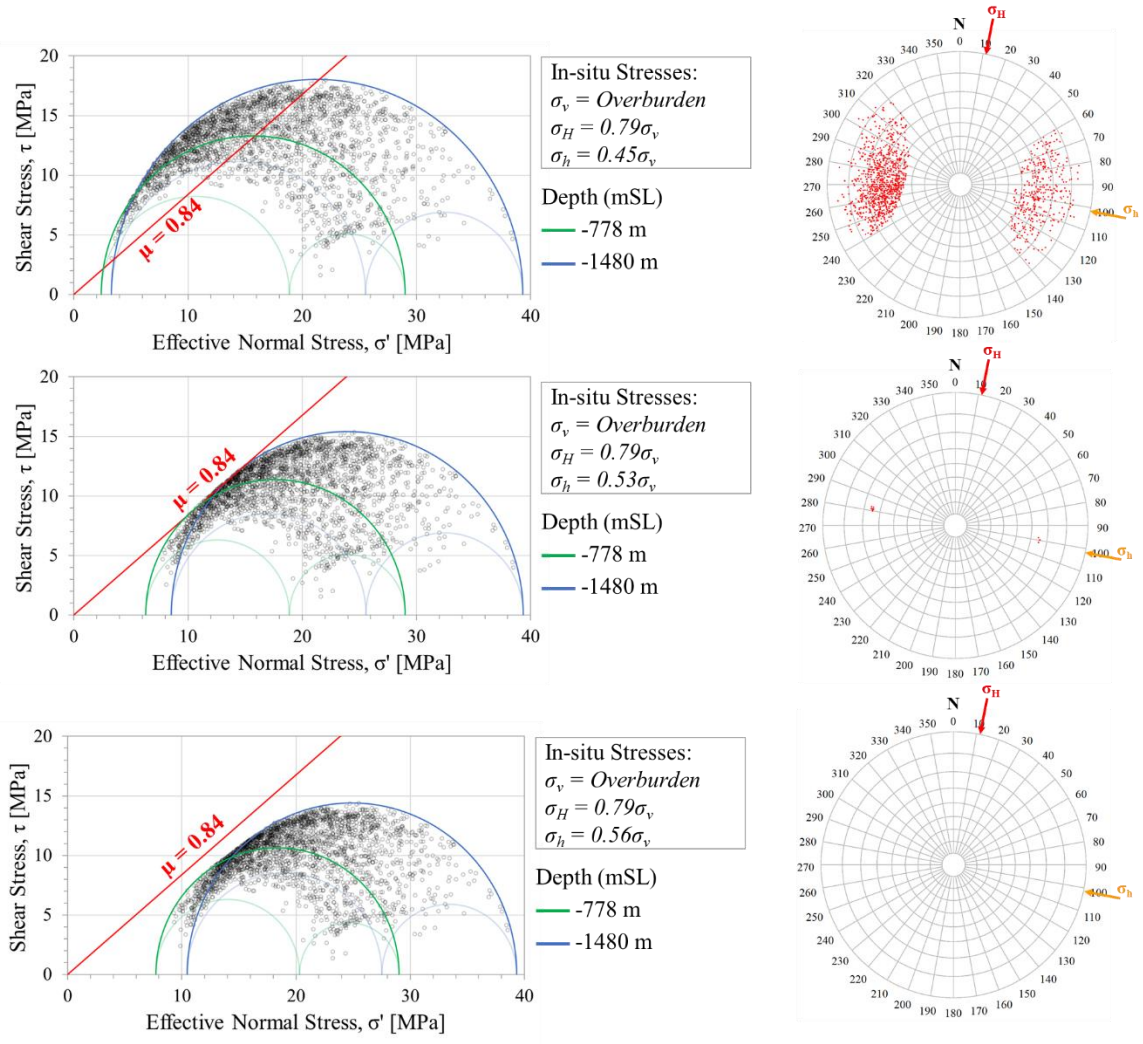

Figure 8: Slip analysis on fracture planes measured from FOH-3D at -778 to -1480 mSL (below mean Sea Level). Top: Slipping fractures shown in red on a stereneot given that σ_h is 0.45σ_v. Middle: The limit of slipping fractures shown in red on the stereneot given that σ_h is 0.53σ_v. Bottom: No fractures slip given that σ_h is 0.56σ_v.

3.3 Constraining the Horizontal In-situ Stresses

Given a lower bound of the minimum in-situ horizontal stress (σ_h) from the slip analysis in Section 3.2, the lower bound of the maximum in-situ horizontal stress (σ_H) can be estimated based on the breakout stability analysis described in Section 3.1. Figure 9 shows that the lower bound of the maximum horizontal in-situ stress is 0.79σ_v. Any values less then this will not produce an acceptable match between the locations of calculated and observed breakouts. An acceptable match was assumed to be within 5% of the observed breakouts depth (2300 m vertical depth). The discontinuation in the logged breakouts at 2500 m vertical depth in Figure 9 was neglected and assumed to be due to a change in rock properties.

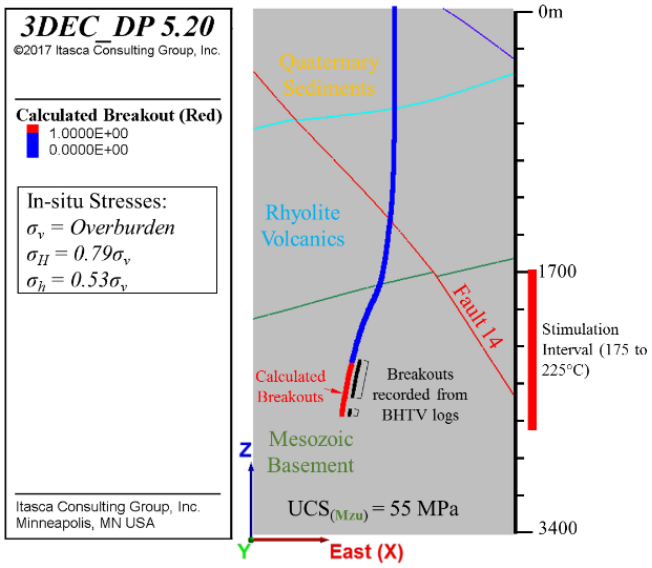

Figure 9: Breakout stability analysis comparing calculated breakouts (red) with ATV recorded breakouts (off-set in black). The least possible value the minimum horizontal stress can be was determined from the slip analysis in Section 3.2. If $\sigma_h = 0.53\sigma_v$ the breakout stability analysis shows an acceptable match between calculated breakouts and observed breakouts when $\sigma_H = 0.79\sigma_v$.

Determining the upper bounds of the minimum and maximum horizontal in-situ stresses requires iterating through the breakout stability analysis holding one of the independent variables constant (σ_h), and incrementing the other variable (σ_H), or visa-versa. The increment chosen had a step size of 0.01 resulting in 594 total solutions. A parameter space matrix detailing the incremental solutions is shown in Figure 10 with red lines mapping the stress space that produces a breakout match with an error less than 5%.

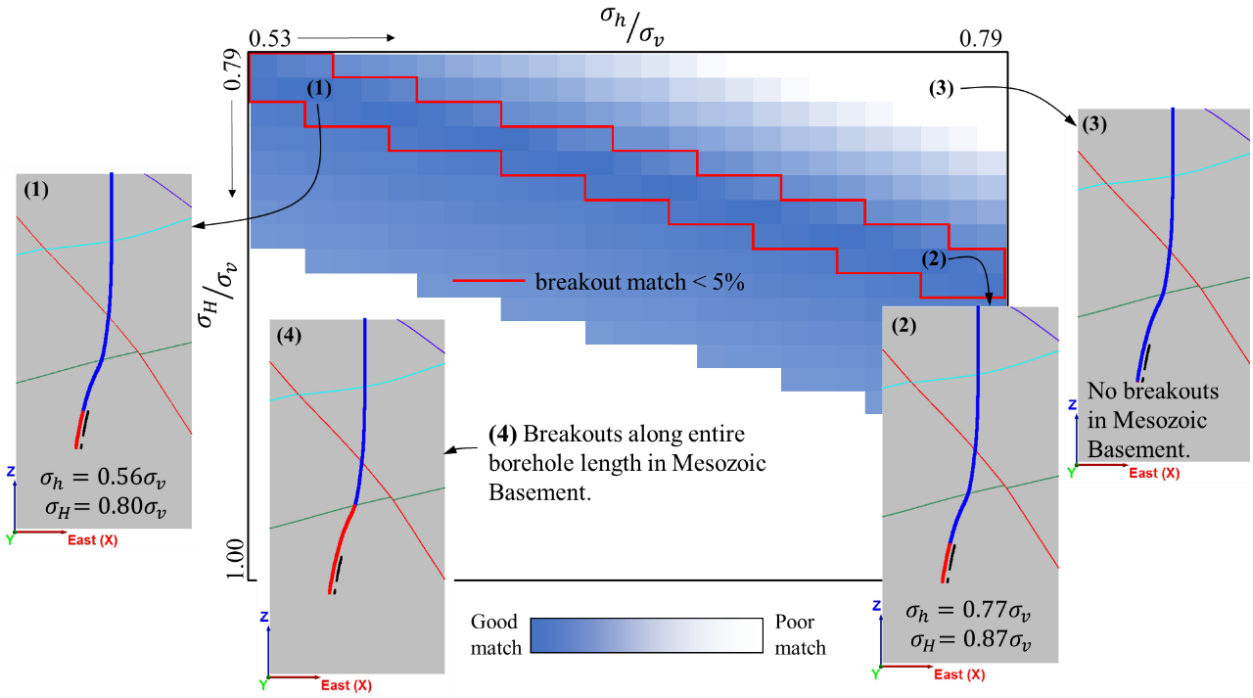

Figure 10: Breakout stability analyses for all possible values $0.53 \leq \sigma_h \leq 0.79$ and $0.79 \leq \sigma_H \leq 1.0$. The darker blue colors represent better matches between calculated breakout locations and breakouts recorded from ATV logs. Four different scenarios are presented: (1) $\sigma_h = 0.56\sigma_v$ and $\sigma_H = 0.80\sigma_v$ shows an acceptable match between calculated and observed breakouts. (2) $\sigma_h = 0.77\sigma_v$ and $\sigma_H = 0.87\sigma_v$ shows an acceptable match between calculated and observed breakouts. (3)

A region (shown in white) where σ_h is too large to allow a breakout to form. (4) A region (shown in white) where σ_H is so large breakouts occur along the entire length of the borehole in the Mesozoic basement rock.

The breakout stability analysis produces the upper and lower bounds on the minimum and maximum horizontal in-situ stresses. These ranges were determined to be:

$$0.53 \leq \sigma_h \leq 0.79$$
$$0.79 \leq \sigma_H \leq 0.88$$

3.4 Comparison with Nearby Stress Measurements

A nearby stress measurement was conducted by means of a "mini frac" test to determine the minimum horizontal in-situ stress, e.g. Hickman and Davatzes (2010). At a depth of approximately 930 meters the minimum horizontal stress was measured to be 61% of the vertical stress. An additional study was also conducted utilizing fault data in the Basin-and-Range province of western Nevada to help inform the magnitudes of the in-situ stresses, e.g. Jolie et al. (2015). This study investigated three different in-situ stress scenarios to help determine favorable drilling orientations. Figure 11 shows the stress profile as a function of depth for these studies and the in-situ stress range determined from the FOH-3D borehole analysis.

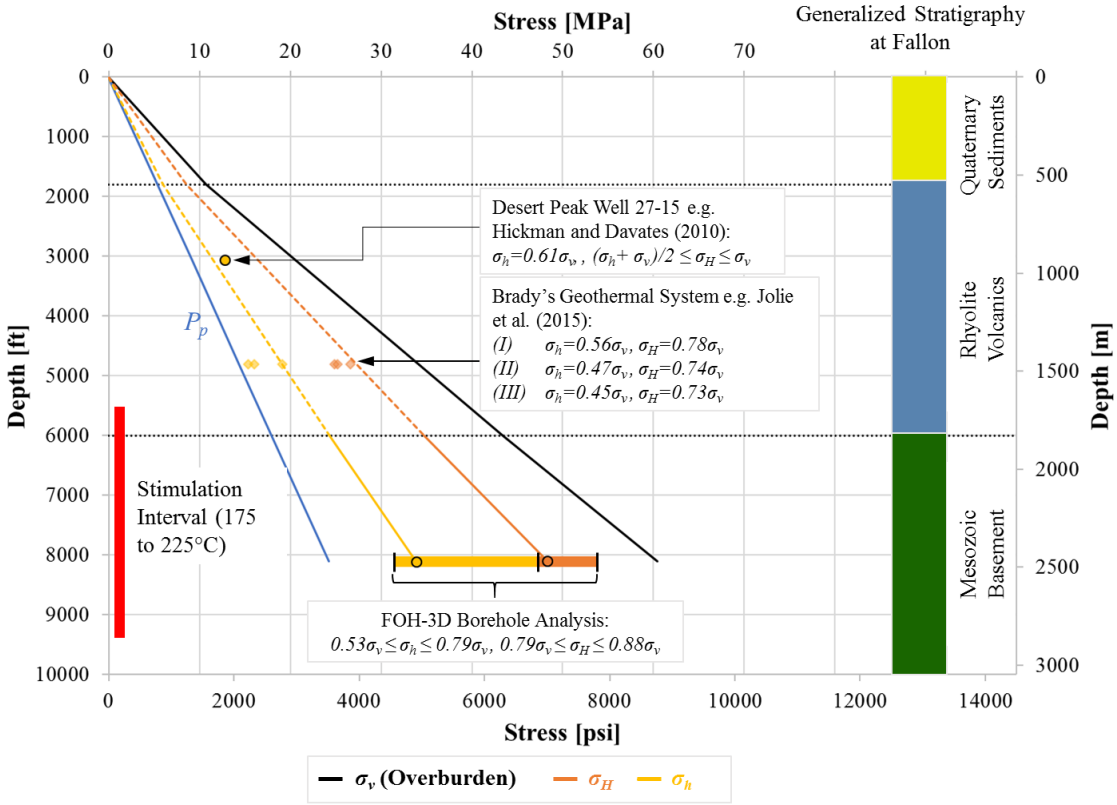

Figure 11: Stress profile generated from FOH-3D borehole data in the Mesozoic basement. Additional stress measurements and values used in nearby studies are shown for comparison.

Based on nearby measurements, we conclude that the best estimate of minimum horizontal stress is equal to 56% of the vertical stress. This estimation was largely motivated by the measurement of σ_h obtained from Hickman and Davates (2010) and the *Scenario I* stress state used in Jolie et al. (2015). Since it was determined $\sigma_h = 0.56\sigma_v$, the corresponding maximum horizontal in-situ stress can be determined from Figure 10. The resulting best estimation for the horizontal in-situ stresses are:

$$\sigma_h = 0.56\sigma_v$$
$$\sigma_H = 0.80\sigma_v$$

4. CONCLUSION

The estimation of in-situ stresses at the Fallon FORGE site by means of FOH-3D breakout and fracture orientations yielded a range of possible values for the minimum and maximum horizontal in-situ stresses. The primary assumptions made in this analysis are that the site is subjected to a normal faulting regime, the friction coefficient on pre-existing fractures is 0.84, and the UCS of the Mesozoic basement rock was 55 MPa. The breakout stability analysis does show that higher values of horizontal stresses are possible. Only by comparison with nearby stress measurements can we make an informed decision as to which side of the range the true stress magnitudes occupy. If no measurements were present, one could reasonably argue the minimum horizontal stress could be any value from 53% to 79% of the vertical stress, the latter of which might suggest the faulting regime moves toward a strike-slip regime or a combination of strike-slip and normal faulting.

As noted earlier, the UCS of the rock used in this study could be considered a small value when compared to other hard rock. It was also shown through indirect measurements that the UCS range in the Mesozoic basement rock was 70 to 200 MPa. However, in our study it was determined that any UCS greater than approximately 90 MPa would not produce any breakouts in the Mesozoic basement, regardless of the magnitudes of the horizontal in-situ stresses. Figure 12 shows the breakout stability analysis for a UCS equal to 70 and 90 MPa. Recall that any white region in the matrix indicates that the current horizontal stresses would not produce breakouts that compare to the observed breakouts.

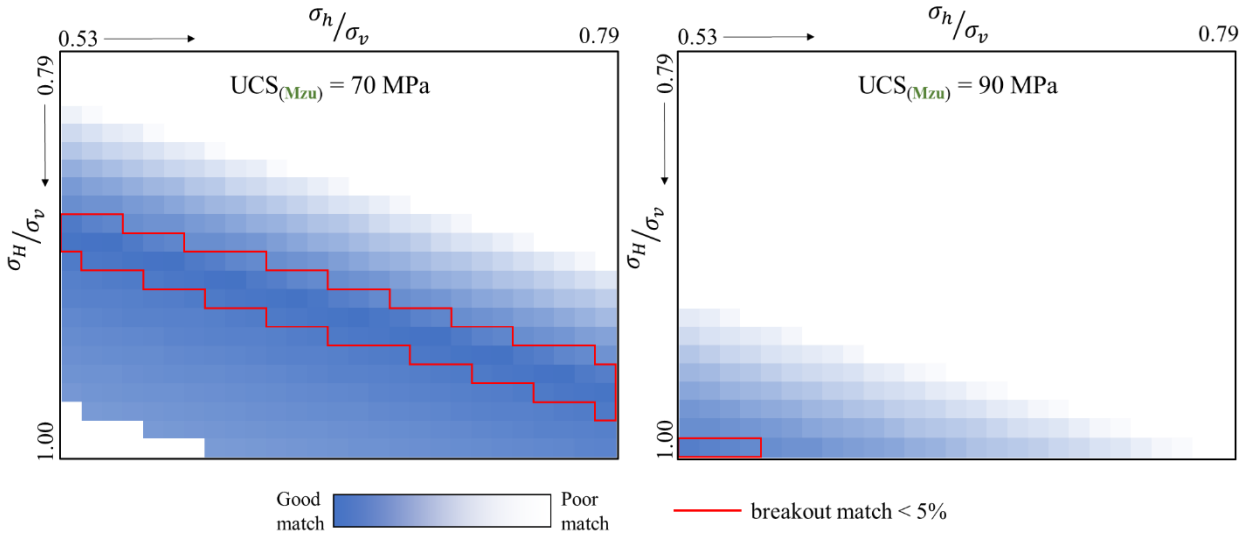

Figure 12: Breakout stability analysis for two different rock strengths. Left: UCS = 70 MPa – Breakout matches with BHTV logs within 5% are outlined in red. Right: UCS = 90 MPa – Breakout matches with BHTV logs within 5% are outlines in red.

We can see that much higher maximum horizontal in-situ stresses (σ_H) are required to produce breakouts when considering higher rock strengths. In fact, if the UCS exceeds 90 MPa the potential for a breakout to form becomes zero at the depth where breakouts were observed. Given these results, a UCS of 55 MPa was considered appropriate for our analysis.

REFERENCES

Blake, K., Davatzes, N.: Borehole Image Log and Statistical Analysis of FOH-3D, Fallon Naval Air Station, NV, *Proceedings*, 37th Workshop on Geothermal Reservoir Engineering, Stanford University, Stanford, CA (2012).

Byerlee, J.D.: Friction of Rock, *Pure Applied Geophysics*, **116**, (1978), 615-626.

Deere, D.U., Miller, R.P.: Engineering Classification and Index Properties for Intact Rock, *Technical Report*, AFWL-TR-65-116, Air Force Weapons Laboratory Research and Technology Division, Kirtland Air Force Base, NM (1966).

Fairhurst, C.: Methods of Determining In Situ Rock Stresses at Great Depths, *Technical Report*, TRI-68, Mo. River Div. Corps of Eng., Omaha, NB (1967).

Hayes, D.: The In-situ Determination of the Complete State of Stress in Rock: The Principles of a Proposed Technique, *CSIR Report*, MEG 404, Counc. for Sci. and Ind. Res., Pretoria, South Africa (1965).

Hickman, S.H., and Davatzes, N.C.: In-situ Stress and Fracture Characterization for Planning of an EGS Stimulation in the Desert Peak Geothermal Field, Nevada, *Proceedings*, 35th Workshop on Geothermal Reservoir Engineering, Stanford University, Stanford, CA (2010).

Hiramatsu, Y., and Oka, Y.: Stress Around a Shaft or Level Excavated in Ground with a Three-dimensional Stress State, *Mem. Fac. Eng. Kyoto Univ.*, **XXIV(I)**, (1962), 56-76.

Jaeger J., Cook, N and Zimmerman, R.: Fundamentals of Rock Mechanics, 4th ed., 219 pp., Blackwell Publishing, Malden, MA, (2007).

Jolie, E., Moeck, I., and Faulds, J.E.: Quantitative Structural – Geological Exploration of Fault-controlled Geothermal Systems – A Case Study from the Basin-and-Range Province, Nevada (USA), *Geothermics*, **54**, (2015), 54-67.

Kirsch, G.: Die Theorie der Elasticitaet und die Bedufnisse der Festigkeitslehre, *VDIZ*, **42**, (1898).

Lutz, S., Hickman, S., Davatzes, N., Zemach, E., Drakos, P., and Robertson-Tait, A.: Rock Mechanical Testing and Petrologic Analysis in Support of Well Stimulation Activities at the Desert Peak Geothermal Field, Nevada, *Proceedings*, 35th Workshop on Geothermal Reservoir Engineering, Stanford University, Stanford, CA (2010).

Lutz, S., Zutshi, A., Robertson-Tait, A., Drakos, P., Zemach, E.: Lithologies, Hydrothermal Alteration, and Rock Mechanical Properties in Wells 15-12 and BCH-3, Bradys Hot Springs Geothermal Field, Nevada, *GRC Transactions*, **32**, (2011).

Mastin, L.: Effect of Borehole Deviation on Breakout Orientations, *Journal of Geophysical Research*, **93**, (1988), 9187-9195.

Moos, D., and Zoback, M.: Utilization of Observations of Well Bore Failure to Constrain the Orientation and Magnitude of Crustal Stresses: Application to Continental, Deep Sea Drilling Project, and Ocean Drilling Program Boreholes, *Journal of Geophysical Research*, **95**, (1990), 9305-9325.

Peska, P., and Zoback, M.D., Compressive Failure of Inclined Well Bores and Determination of In Situ Stress and Rock Strength, *Journal of Geophysical Research*, **100**, (1995), 12791-12811.

Qian, W., and Pedersen, L.: Inversion of Borehole Breakout Orientation Data, *Journal of Geophysical Research*, **96**, (1991), 20093-20107.

Zajac, B., and Stock, J.: Using Borehole Breakouts to Constrain the Complete Stress Tensor: Results from the Sijan Deep Drilling Project and Offshore Santa Maria Basin, California, *Journal of Geophysical Research*, **102**, (1997), 10083-10100.

Zoback, M., Barton, C.A., Brudy, M., Castillo, D.A., Finkbeiner, T., Grollimund, B.R., Moos, D.B., Peska, P., Ward, C.D., Wiprut, D.J. : Determination of Stress Orientation and Magnitude in Deep Wells, *International Journal of Rock Mechanics & Mining Sciences*, **40**, (2003), 1049-1076.

Zoback, M., Moos, D., and Mastin, L.: Well Bore Breakouts and In Situ Stress, *Journal of Geophysical Research*, **90**, (1985), 5523-5530.